IEEE Access
Multidisciplinary | Rapid Review | Open Access Journal

Received June 3, 2020, accepted June 14, 2020, date of publication June 29, 2020, date of current version July 13, 2020.

Digital Object Identifier 10.1109/ACCESS.2020.3005439

Fractional Controller Design of a DC-DC Converter for PEMFC

ZHIDONG QI, JUNTAO TANG, JIN PEI, AND LIANG SHAN
School of Automation, Nanjing University of Science and Technology, Nanjing 210094, China

Corresponding author: Juntao Tang (2484732155@qq.com)

This work was supported in part by the National Natural Science Foundation of China under Grant 61374153, and in part by the Jiangsu Provincial Nature Science Foundation under Grant BK20191286.

ABSTRACT Proton Exchange Membrane Fuel Cell (PEMFC) is difficult for application because of its high current and wide voltage output. A fractional order PID controller is introduced to a Four-Switch Buck-Boost DC/DC converter to stabilize the power output in this paper. To reduce the inductor current ripple, a kind of dual-triggered switch strategy is employed in detail, and an accurate dynamic model of DC/DC converter is proposed for fuel cell measurement and control system. Then a fractional order PID controller is designed for voltage module compensation, in which a stochastic inertia weight PSO algorithm is employed to optimize the parameters of this controller. The results of simulation and experiment indicate that the compensation effect of fractional order PID controller has better performance than the integer order controller, which is robust to the variation of fuel cell system dynamics and power request.

INDEX TERMS Four-switch buck-boost converter, fractional order PID controller, PEMFC.

I. INTRODUCTION

Proton Exchange Membrane Fuel Cell (PEMFC) is one of the best power generation devices for the civilian application of hydrogen energy, which has the advantages of high efficiency, no pollution, low operating temperature, and has great application prospects[1]. However, as affected by the inner electrochemical reaction, the output characteristics of PEMFC will be a fluctuating cell voltage. It is necessary to employ a DC-DC converter to pre-stabilize the output voltage to create conditions for further power conversion in the subsequent stage[2].

PEMFC power conversion unit is a non-negligible part of the entire system, and the improvement and control of front-end DC-DC converter in the two-stage PEMFC power generation system has become a popular research topic. At present, scholars have proposed various topological structures, which can be divided into two main types: isolated and non-isolated. Isolated DC-DC converters generally have a DC-AC-DC structure, in which high-frequency transformers including forward and flyback converters are often used to fulfill the isolation function. However, due to low utilization and magnetic reset circuits, high-frequency transformers will make the design more difficult and affect the efficiency of the entire unit, which is less used in PEMFC power generation systems. As to the non-isolated DC-DC converts, Buck-Boost converter is usually employed to achieve step-up or step-down function, but its output and input voltage have opposite polarity. Therefore, scholars have proposed a variety of non-isolated Buck-Boost circuits. Shiluveru *et al.* [3] added q-ZSC(quasi-Z-source converter) topology to traditional Buck-Boost converter, which can realize power conditioning with improved reliability along with inherent shoot-through protection capability. Liangjing [4] introduced soft-switching units to the control of Buck-Boost converter, whose results indicate that it can effectively reduce switching losses. Wenbo [5] proposed a new Three-Port converter, which combines Buck-Boost converter with dual-active bridge converter and conclude that it can realize flexible step-up or step-down and bidirectional power flow. Yafei [6] put forward a non-inverting Buck-Boost converter to prove that it can convert a wide range of energy storage terminal voltage into a constant output voltage of the DC bus, greatly improving power supply capacity of the energy storage unit. Wangyu [7] added NQ60 Buck-Boost module to a program-controlled DC/DC converter to avoid the shortage of direct power supply of the energy storage battery, whose efficiency can reach about 94%. Xiaofeng *et al.* [8] proposed a control scheme of achieving zero-voltage-switching(ZVS) for the non-isolated three-level

The associate editor coordinating the review of this manuscript and approving it for publication was Valentina E. Balas.

Buck-Boost converter, but it required multiple switches and multiple sets of control circuits, which increased the complexity and cost of the entire system. Xiaoli [9] adopted Four-Switch Buck-Boost converter under multi-mode control which is applied to a fuel cell system to confirm that it can respectively reduce voltage stress of switching devices and improve switching power supply's level. However, all of these converters were designed with integer order controller, which may not be suitable for PEMFC system with fractional order characteristics [10]. Here, a Four-Switch Buck-Boost converter with fractional order controller will be employed to stabilize PEMFC output voltage and improve the converter efficiency.

Proton exchange membrane fuel cell is a multi-input, multi-output and non-linear time-varying system, whose output characteristics are difficult to control due to the influence of multiple parameters. Scholars and experts have proposed various control methods to control PEMFC dynamic output from different angles in order to improve the cell power. Zhanli *et al.* [11] used a traditional PID algorithm controller to control the output current of the converter by analyzing the impact of the step change of the output current on the output voltage, output power and efficiency, which proved that the designed algorithm attained better robustness and greatly improved the performance of PEMFC system. Haojie *et al.* [12] designed a sliding mode control circuit of PEMFC-Boost converter system to realize the effective control of the nonlinear behavior and improve the system output performance. Compared this sliding mode control with a general PI control by simulation, it was obvious that sliding mode control strategy could well stabilize output voltage of the system. Jun *et al.* [13] designed a continuous model predictive controller (CMPC) by employing Laguerre functions and proposed a simple modification strategy by appling an index weighting function, and the simulation results showed the system with CMPC had good response characteristics and robustness, achieving constant output power of PEMFC. Although pre-regulation and anti-interference can be achieved by these control strategies to a certain extent, they all neglect the essential fractional-order characteristics of PEMFC.

As a matter of fact, several processes including gas diffusion, thermal diffusion and convection diffusion in PEMFC all have typical fractional order properties [14]. Hongliang [15] proved that the fuel cell EIS diagram was an inferior arc rather than a complete semi-circular arc for integer system, which showed that fuel cell has fractional order characteristic. Zhidong *et al.* [16] proposed a fractional order Hammerstein model identification algorithm, whose results could accurately describe the output characteristics of the stack, which meant that the fractional order peculiarity in PEMFC couldn't be ignored. Based on the fractional order model of Buck converter, Huili *et al.* [17] proposed a fractional order $PI^{\lambda}D^{\mu}$ control method, and constructed a voltage-controlled fractional order Buck converter feedback control system. And it is obvious that the FOPID controller has better performance and the proposed control strategy for fractional order Buck converter is strongly robust to the disturbance of input voltage. Xiuhui *et al.* [18] employed the fractional calculus theory to model the original Boost converter system, and replaced the integer order PID controller with a fractional order PID controller to obtain better system performance, whose results indicate that the fractional order model can describe characteristics of the Boost converter more accurately. Considering PEMFC and its converter as an entire system with fractional characteristic, in this paper, a fractional order PID controller is employed to fulfill the cell's voltage module compensation, in which a stochastic inertia weight PSO algorithm is adopted to optimize the parameters of the controller.

This paper is organized as follows. In Section II, a more accurate dynamic model of the converter will be established based on the topology evolution and working principle of Four-Switch Buck-Boost converter. Section III will provide the controller design of PEMFC regulated voltage module, including an integer order controller and a fractional order controller. In Section IV, the performance of different controllers will be compared based on the cascaded simulation model of PEMFC and Four-Switch Buck-Boost converter built in Simulink. In Section V, the Tustin with PSE method is used to discretize the fractional order PID controller. In Section VI, a 50W experiment prototype is adopted to verify the actual application effect of the fractional order PID controller under different working conditions. Finally, this paper will be concluded in Section VII. Compared with the integer order controller, the fractional order PID controller acquires more excellent performance, which means that the dynamic response has small overshoot, short settling time, small steady state ripple and acceptable error range.

II. ANALYSIS AND DYNAMIC MODELING OF PEMFC PRE-STAGE POWER CONVERTER

Compared with traditional DC chopper circuits, Four-Switch Buck-Boost(FSBB) converter has fewer passive components, lower device stress and simple structure, and it is more suitable to be employed as the DC-DC power converter of PEMFC which has large current and wide-range voltage output.

A. WORKING PRINCIPLE

FSBB converter is a simplified structure shown in Figure 1 from the concatenation of Buck and Boost converter by removing the intermediate capacitance and associating with two inductors.

Where Q_1,Q_{sr1} is Buck group switch whose duty cycle is D_1 and 1-D_1, respectively, while Q_2,Q_{sr2} is Boost group switch whose duty cycle is D_2 and 1-D_2, respectively. Under steady-state operating condition, the volt-second balance equation for points A and B can be obtained as follows, in which V_{in} is the input voltage and V_{out} is the output voltage.

$$V_{in} \cdot D_1 = V_{out} \cdot (1 - D_2) \tag{1}$$

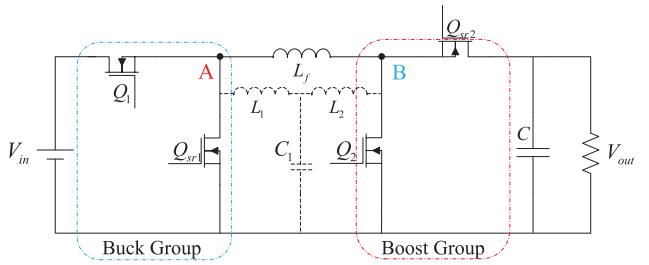

FIGURE 1. Four-Switch Buck-Boost converter.

(1) can be reduced to

$$\frac{V_{out}}{V_{in}} = \frac{D_1}{1 - D_2} \tag{2}$$

Two independent degrees of freedom are easier to achieve high gain in a given range and make the control process more flexible. When $D_1 + D_2 < 1$, the converter works in Buck mode, otherwise in Boost mode.

B. COMPARISON OF DIFFERENT SWITCH TRIGGER STRATEGIES

The same edge-triggered strategy[19] is usually adopted in multi-switch converter, where T_s represents the cycle time. The inductor current pulsation value can be denoted by:

$$\Delta I_{L_f\_one\_s} = \begin{cases} \dfrac{V_{out}(1 - D_1)T_s}{L_f}, & V_{in} \geq V_{out} \\ \dfrac{D_2 V_{in} T_s}{L_f}, & V_{in} < V_{out} \end{cases} \tag{3}$$

However, the dual-triggered strategy proposed by REN[20] can further reduce the converter loss, in which the two switches are modulated at the leading edge and trailing edge respectively. The steady-state waveform of FSBB converter with dual-triggered strategy is shown in Figure 2.

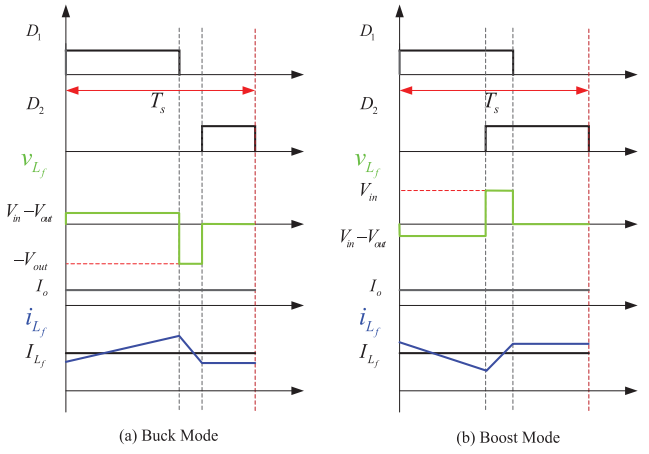

FIGURE 2. The steady-state waveform with dual-triggered strategy.

There are three levels of inductor L_f voltage,$V_{in} - V_{out}$, $-V_{out}$ and 0 in the dual edge regulation process. Compared with the same edge-triggered strategy, the switches have lower voltage stress, and the reduction of the inductor voltage amplitude can effectively reduce the inductor current ripple and switching power supply volume.

The inductor current pulsation value with dual-triggered strategy can be expressed as:

$$\Delta I_{L_f\_one\_d} = \begin{cases} \dfrac{V_{out}(1 - D_1 - D_2)T_s}{L_f}, & V_{in} \geq V_{out} \\ \dfrac{(D_1 + D_2 - 1)V_{in}T_s}{L_f}, & V_{in} < V_{out} \end{cases} \tag{4}$$

If $\Delta I_{L_f} = \Delta I_{L_f\_one\_s} - \Delta I_{L_f\_one\_d}$, then

$$\Delta I_{L_f} = \begin{cases} \dfrac{V_{out} D_2 T_s}{L_f}, & V_{in} \geq V_{out} \\ \dfrac{(1 - D_1)V_{in}T_s}{L_f}, & V_{in} < V_{out} \end{cases} \tag{5}$$

Regardless of step-up or step-down, the inductor current pulsation is small with dual edge triggering strategy, which is helpful to increase the power density of the converter. Therefore, the switch dual-triggered strategy is adopted in this paper.

C. DYNAMIC MODELING OF FSBB CONVERTER

While setting up models of a FSBB converter, the Buck or Boost mode is usually considered separately ignoring the interaction between two working conditions, which cannot describe the dynamic performance completely. In this paper, a accurate dynamic model of FSBB converter is established based on the principle of high frequency switching network equivalence. The detailed steps are as follows: (1)The path of the current sudden change is defined as a branch due to the switch action, which is equivalent to the controlled current source. (2)The point where the voltage abrupt changes is defined as a node, which is equivalent to the controlled voltage source. (3)The controlled value is equivalent to the arithmetic mean value of the previous-cycle current or voltage. The switching network equivalent model of FSBB converter is shown in Figure 3.

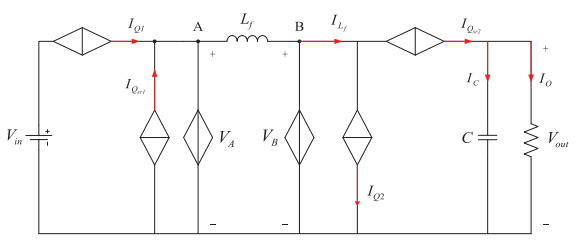

FIGURE 3. The switching network equivalent model of FSBB converter.

The steady state of the model can be expressed as:

$$\begin{cases} I_{Q_1} = I_{L_f} \cdot D_1 \\ I_{Q_{sr1}} = I_{L_f} \cdot (1 - D_1) \\ I_{Q_2} = I_{L_f} \cdot D_2 \\ I_{Q_{sr2}} = I_{L_f} \cdot (1 - D_2) \\ V_A = V_{in} \cdot D_1 \\ V_B = V_{out} \cdot (1 - D_2) \end{cases} \tag{6}$$

In order to study the dynamic characteristics of the converter, it is necessary to introduce perturbation to the various variables:

$$x = \hat{x} + X \tag{7}$$

Then, the dynamic expression of FSBB converter model can be denoted as:

$$\begin{cases} D_1 + \hat{d}_1 = d_1 \\ D_2 + \hat{d}_2 = d_2 \\ V_A + \hat{v}_A = v_A \\ V_B + \hat{v}_B = v_B \\ I_{Q_1} + \hat{i}_{Q_1} = i_{Q_1} \\ I_{Q_{sr1}} + \hat{i}_{Q_{sr1}} = i_{Q_{sr1}} \\ I_{Q_2} + \hat{i}_{Q_2} = i_{Q_2} \\ I_{Q_{sr2}} + \hat{i}_{Q_{sr2}} = i_{Q_{sr2}} \\ V_{in} + \hat{v}_{in} = v_{in} \\ V_{out} + \hat{v}_{out} = v_B \\ I_{L_f} + \hat{i}_{L_f} = i_{L_f} \end{cases} \tag{8}$$

Equation(8) can be linearized by removing the high-order terms to get FSBB converter equivalent incremental topology shown in Figure 4.

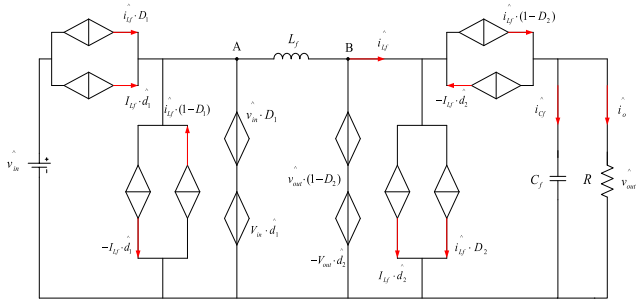

FIGURE 4. Equivalent incremental topology of FSBB converter.

From Figure 4, the KVL equation that describes the converter dynamic characteristics is straight-forwardly derived as follows:

$$L_f \frac{di_{L_f}}{dt} + [-V_{out} \cdot \hat{d}_2 + \hat{v}_{out} \cdot (1 - D_2)] = V_{in} \cdot \hat{d}_1 + \hat{v}_{in} \cdot D_1 \tag{9}$$

Meanwhile, the KCL equation can be acquired as well:

$$C_f \frac{d\hat{v}_{out}}{dt} + \frac{\hat{v}_{out}}{R} = -I_{L_f} \cdot \hat{d}_2 + \hat{i}_{L_f} \cdot (1 - D_2) \tag{10}$$

At zero initial state, the derived duty cycle-to output voltage transfer function under Buck mode ($\hat{v}_{in} = 0, \hat{d}_2 = 0$) by Laplace transforming is expressed as:

$$G_{d_1 v_o}(s) = \frac{\hat{v}_{out}(s)}{\hat{d}_1(s)} = \frac{V_{in}(1 - D_2)}{L_f C_f s^2 + \frac{L_f}{R} s + (1 - D_2)^2} \tag{11}$$

The derived duty cycle-to-output voltage transfer function under Boost mode ($\hat{v}_{in} = 0, \hat{d}_1 = 0$) is expressed as:

$$G_{d_2 v_o}(s) = \frac{\hat{v}_{out}(s)}{\hat{d}_2(s)} = \frac{V_{out}(1 - D_2) - L_f I_{L_f} s}{L_f C_f s^2 + \frac{L_f}{R} s + (1 - D_2)^2} \tag{12}$$

In the previous section, the advantages of the dual-triggered strategy have been clearly described, and the difficulty of the hardware and software design will be increased with two sets of duty cycle control methods. Let $D_1 = D_2 = D$, then the influence of the change of duty ratio on the output voltage ($\hat{v}_{in} = 0$)can be unified as follows:

$$G_{dv_o}(s) = \frac{\hat{v}_{out}(s)}{\hat{d}(s)} = \frac{(V_{in} + V_{out})(1 - D) - L_f \frac{V_{out}}{R(1 - D)} s}{L_f C_f s^2 + \frac{L_f}{R} s + (1 - D)^2} \tag{13}$$

III. DESIGN OF PEMFC PRE-REGULATION MODULE CONTROLLER

The closed loop design block diagram of the typical switching power supply is presented in Figure 5.

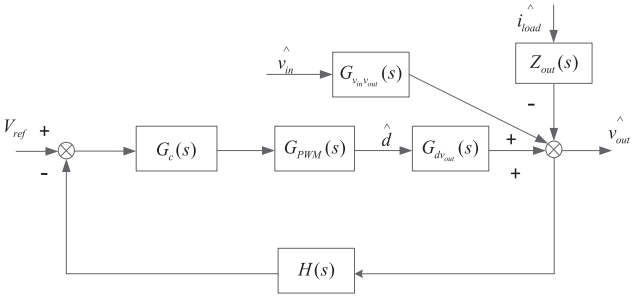

FIGURE 5. Closed loop structure of system.

The loop gain of the DC-DC converter is expressed as:

$$T(s) = G_c(s) G_{PWM}(s) G_{dv_0}(s) H(s) \tag{14}$$

where $G_c(s)$ and $H(s)$ is the designed controller and feedback transfer function, respectively. $G_{PWM}(s) = 1/V_M$, V_M is the carrier amplitude. Table 1 presents details of FSBB converter specifications.

If $G_{dv_{out}}(s) = \hat{v}_{out}(s)/\hat{d}(s)$, when the minimum input voltage is 16V, the theoretical duty cycle is 0.6, the controlled object of closed loop design under Boost mode is given by:

$$G_{dv_{out}}(s) = \frac{16 - (5e - 5)s}{(1e - 9)s^2 + (8.33e - 7)s + 0.16} \tag{15}$$

TABLE 1. Converter specification.

Parameter	Value
Input voltage	16 to 30V
Output voltage	24V
f_s	100kHz
Typical load	12 Ω
L_f	10 μH
C_f	100 μF

When the maximum input voltage is 30V, the theoretical duty cycle is 0.44, the controlled object of closed loop design under Buck mode is expressed as:

$$G_{dv_{out}}(s) = \frac{30 - (3.6e-5)s}{(1e-9)s^2 + (8.33e-7)s + 0.3136} \tag{16}$$

The system bode diagram of these two limit input voltages without compensation is shown in Figure 6.

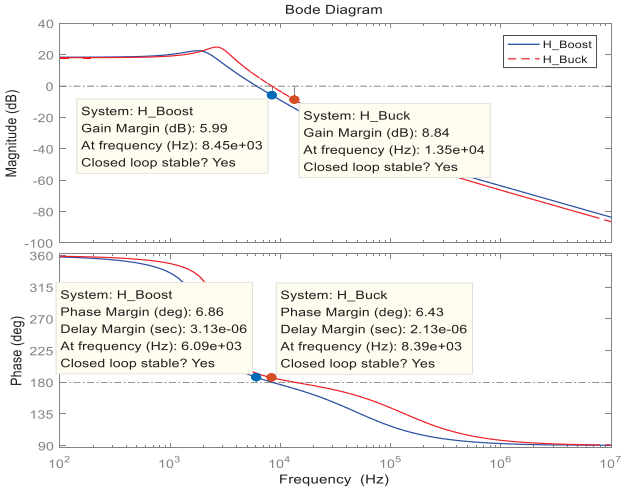

FIGURE 6. Frequency response for FSBB converter without compensation.

In the bode diagram, the performance of two working modes is very close. As there is a zero point in the right half plane, the phase frequency characteristic curve is distorted, and the phase margin is not high: 6.86°and 6.43° respectively. Meanwhile, the slope of phase margin in the vicinity of the crossing frequency is large, indicating that the anti-interference ability of the system is not strong. It is necessary to further compensate the system for good results. In this paper, Buck mode (H _ Buck) is selected to design the closed loop compensator.

A. DESIGN OF INTEGER ORDER CONTROLLER

FSBB converter is a non-minimum phase system, the relationship between the phase frequency characteristic curve and the performance is not clear. In this paper, based on the typical design method[21], a Two-Zero/Three-Pole(TZTP) compensator devised for the controlled object with right half plane zero point is proposed as:

$$G_c = \frac{(1 + 0.0001137s)(1 + 0.0001137s)}{0.000269s(1 + 0.0000012s)(1 + 0.0000012s)} \tag{17}$$

Apparently, TZTP controller belongs to integer order controller, and the system bode diagram with compensation is shown in Figure 7.

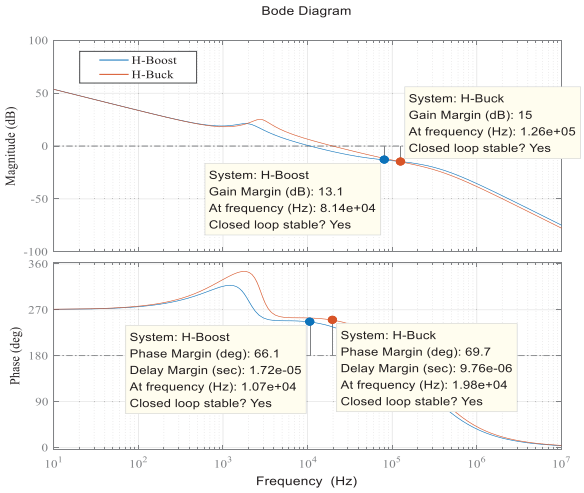

FIGURE 7. Frequency response for FSBB converter with compensation.

From Figure 7, the phase and gain margin of the system with a TZTP compensator are improved after compensation, which are bigger than 65°and about 15dB, respectively. The anti-interference ability of the system has almost reached the design target of closed loop.

B. DESIGN OF FRACTIONAL ORDER CONTROLLER

For the system with fractional-order characteristics, the integer order controller is hard to get good performance. It must be a better selection to study the practical application of a fractional order controller, which shows stronger robustness in related industrial fields. Bouakkaz *et al.* [22] proposed an adapted control strategy where the PV voltage is regulated by a fractional order PID controller in various regions and it can be seen that the proposed dynamic performance improvement strategy has excellent transient responses in different operating scenarios and can well improve the PV system dynamics. Kommula and Kota [23] put forward a Firefly Algorithm (FA) based Fractional Order PID (FOPID) Controller for Brushless DC (BLDC) motor to achieve an effective control of torque and speed and it is obvious that the FOPID torque controller controls the motor torque effectively with a very low ripple from simulation results. At present, mature fractional order controllers mainly include fractional order PID controller, CRONE controller, TID controller and fractional order lead-lag compensator[24]. Compared with other fractional order controllers, the fractional order PID controller has a stronger application potential and its development is relatively mature. Fractional order PID(FOPID) controller proposed by Professor I. Podlubuy[25] is expressed as:

$$G_c(s) = K_p + \frac{K_i}{s^\lambda} + K_d s^\mu \tag{18}$$

Unlike traditional PID controller, the FOPID controller has two more adjustable parameters (integral order λ and differential order μ), which will make the controller more flexible, but increase the difficulty of parameter adjusting. It has been proved that $PI^{\lambda}D^{\mu}$ controllers have advantages in terms of stability and dynamic performance. In this paper, an improved PSO is proposed to adjust FOPID controller parameters. The traditional PSO[26] algorithm was developed by Kennedy and Eberhart in 1995, which got inspired by birds flocking in search of food. The position and velocity of particles are updated as follows:

$$\begin{cases} v_i^{k+1} = w^k v_i^k + c_1 \cdot r_1 \cdot p_i^k + c_2 \cdot r_2 \cdot g_i^k \\ p_i^k = Pbest_i^k - x_i^k \\ g_i^k = Gbest_i^k - x_i^k \\ x_i^{k+1} = x_i^k + v_i^{k+1} \end{cases} \tag{19}$$

where inertia weight(w^k),self-cognitive factor(c_1) and social cognitive factors(c_2) assign the weight to the inertial influence(v_i^k), the personal optimum(p_i^k) and the global optimum(g_i^k). k is the number of current iterations, i represents the number of particles in the population, x_i^k indicates the particle's current position, $Pbest_i^k$ and $Gbest_i^k$ refer to the optimal position of itself and the population respectively during the process, r_1 and r_2 are random numbers between 0 and 1.

In order to avoid the particle falling into the local optimum, a fitness variance is introduced to evaluate the current convergence degree of population, which can dynamically adjust the inertia weight combined with random probability, trying to find the equilibrium point between global search and local search. The particle fitness variance proposed to observe the particle diversity in the iteration process is defined as:

$$D^2 = \sum_{i=1}^{N} \left(\frac{f_{Fitness_i} - f_{avg}}{f_{nor}} \right)^2 \tag{20}$$

where f_{avg},f_{nor} denote the average fitness value of swarm and normalized operator, respectively. f_{avg} can be expressed with the following equation.

$$f_{avg} = \frac{1}{N} \sum_{i=1}^{N} f_{Fitness_i} \tag{21}$$

Meanwhile, f_{nor} is defined by:

$$f_{nor} = \begin{cases} \max\{|f_{Fitness_1} - f_{avg}|\}, & |f_{Fitness_1} - f_{avg}| > 1 \\ 1, & |f_{Fitness_1} - f_{avg}| \le 1 \end{cases} \tag{22}$$

As the variance gets smaller during the optimizing process, the particle will become more concentrated. When the iteration number(C_{Iter}) is less than a threshold(C_s), particles aggregation (D^2 less than d^2) would trigger to adjust the inertia weight w with probability p. p can be expressed as:

$$p = \begin{cases} (C_s - C_{Iter})/C_s, & (C_{Iter} < C_s) and (D^2 < d^2) \\ 0, & others \end{cases} \tag{23}$$

where C_{Iter} and d^2 denote the set maximum number of iterations and the radius of convergence respectively.

Under normal conditions, the inertia weight decreases linearly, which is given by:

$$w^k = \begin{cases} w_{\min} + k \cdot (w_{\max} - w_{\min})/C_{Iter}, & p = 0 \\ r + w^k, & p > r \end{cases} \tag{24}$$

where $w_{\max}$ and $w_{\min}$ are setting intervals for inertia weights, r represents a random number between 0 and 1.

In order to make the control object have good dynamic performance and avoid excessive control excessive control in the optimization process, the weighted integrated time absolute error($ITAE$) and control quantity square is employed as the basic fitness function in this paper. Moreover, a penalty factor C_p is also added to the fitness function by evaluating the value of the overshoot in the system dynamic response. The expression of $ITAE$ will be described as:

$$ITAE = \int_0^t t\,|e(t)|dt \tag{25}$$

And the final Fitness function can be represented as:

$$f_{Fitness} = \begin{cases} \beta_1 \cdot ITAE + \beta_2 \cdot \int |u|^2 dt, & \sigma < 3\% \\ c_p \cdot (\beta_1 \cdot ITAE + \beta_2 \cdot \int |u|^2 dt), & \sigma > 3\% \end{cases} \tag{26}$$

where $\beta_1 + \beta_2 = 1$, c_p is set to 1.5.

Based on PEMFC fractional impedance characteristic model [27] and the above improved PSO algorithm theory, the model of $PI^{\lambda}D^{\mu}$ controller parameter optimization is established in Simulink as shown in Figure 8.

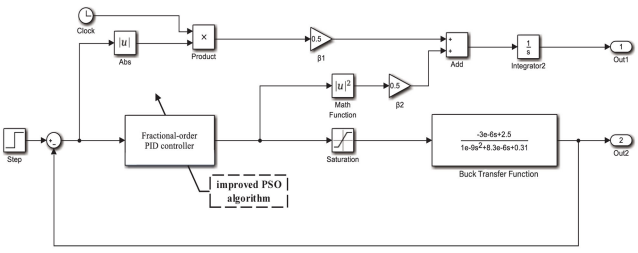

FIGURE 8. $PI^{\lambda}D^{\mu}$ **controller parameter optimization model.**

By multiple optimization, a FOPID controller is attained as follows.

$$G_{FOPID}(s) = 0.008 + \frac{150.3469}{s^{0.99}} + 0.0075s^{0.0087} \tag{27}$$

Compared with equation(18), it is obvious that $K_p = 0.008$, $K_i = 150.3469$ and K_d is set to 0.0075.

IV. SYSTEM SIMULATION

The cascaded simulation model of PEMFC and FSBB converter is built in Simulink and presented in Figure 9. The output voltage response with different controllers is analyzed when the system load varies in this section.

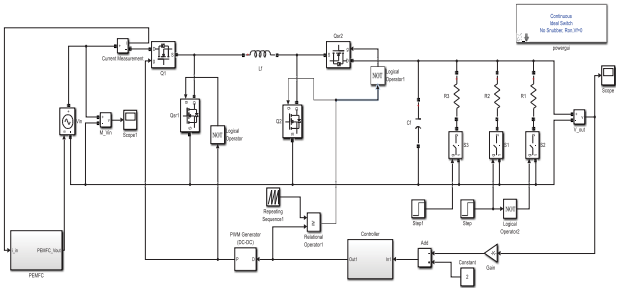

FIGURE 9. The cascaded simulation model of the regulated voltage module.

The closed loop system starts at a rated load ($R = 12\Omega$), then the resistive load increases to 16Ω at 0.5s, decreases to 8Ω at 1s.

The dynamic response is displayed in Figure 10. When the system starts, the response curve compensated by a TZTP controller appears a large overshoot with the shortest rising time, nearly 35%, while the system has no overshoot and can quickly achieve stability with a FOPID controller. When the load varies at 0.5s and 1s, the dynamic curve compensated by a TZTP controller has smaller overshoot and voltage spike than by $PI^{\lambda}D^{\mu}$ controller, which indicates that the adjusting speed of the FOPID controller is not very quick because of its more complicated computing process.

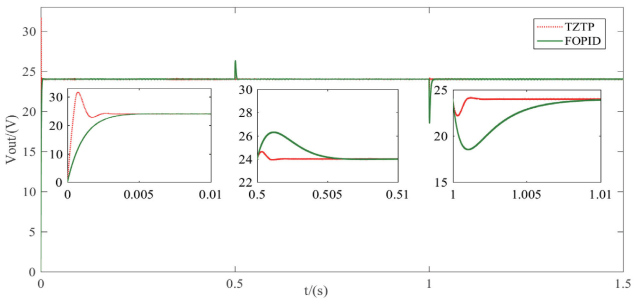

FIGURE 10. The dynamic response curves.

The steady-state ripple of output voltage at rated load is depicted in Figure 11. It is found that the ripple curve compensated by $PI^{\lambda}D^{\mu}$ controller is more ideal than that with obvious "burr" by a TZTP controller. Meanwhile, the steady-state ripple curves of output voltage at 16Ω and 8Ω are shown in Figure 12 and Figure 13 respectively. The output voltage ripple becomes smaller at higher resistive load, and the ripple increases with the output current at lower resistive load. It is found that in accordance with the situation at rated load, the corresponding ripple curve of $PI^{\lambda}D^{\mu}$ controller is more uniform and smooth.

V. DIGITAL REALIZATION OF CONTROLLER

The analog controller $G(s)$ cannot be used directly on the digital platform. It is necessary to discretize the differential equations firstly.

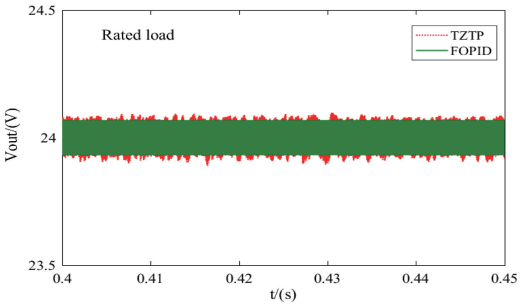

FIGURE 11. The dynamic response curves at rated load.

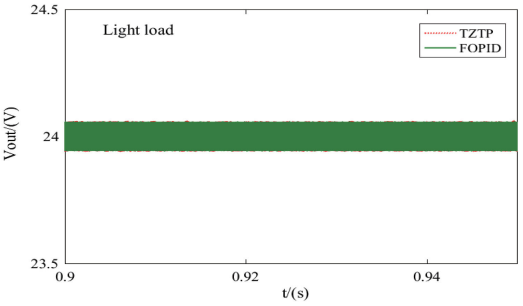

FIGURE 12. The dynamic response curves at 16Ω.

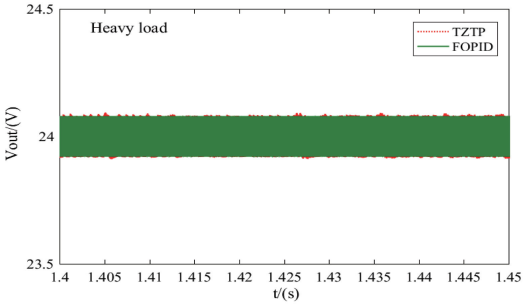

FIGURE 13. The dynamic response curves at 8Ω.

In this paper, the Tustin with PSE method[28] is adopted to discretize the FOPID controller.

(1)Tustin transformation is employed to generate $(\omega(z^{-1}))^n$, which can be expressed as follows.

$$s^n = \left(\frac{2(1-z^{-1})}{T(1+z^{-1})}\right)^n \tag{28}$$

where n represents the rationalized order, T represents the adoption period.

(2)PSE is a method of polynomial approximation after power series expansion, which is given by:

$$D^n(z) = (\omega(z^{-1}))^n = T^n z^{-\left[\frac{L}{T}\right]} \sum_{i=0}^{\left[\frac{L}{T}\right]} (-1)^i \binom{n}{i} z^{\left[\frac{L}{T}\right]-i} \tag{29}$$

where n represents the rationalized order, T represents the adoption period, [] is the rounding operator, and L is the interception length.

When the approximate order of rationalization is 2 and the sampling frequency is 10kHz, the discrete expression of controller is obtained as follows.

$$D(z) = \frac{0.02369 - 0.008594z^{-1} + (6.692e-5)z^{-2}}{1 - 0.9913z^{-1} - 0.0087z^{-2}} \quad (30)$$

The differential equation of the $PI^{\lambda}D^{\mu}$ controller available for programming is:

$$u(k) = 0.02369e(k) - 0.00859e(k-1) + 0.00006692e(k-2) + 0.9913u(k-1) + 0.0087u(k-2)| \quad (31)$$

where $u(k)$ and $e(k)$ represents the controller output and the error input signal respectively.

It is also necessary to discretize the controlled object. Considering the delay characteristics of sampling and other links, the zero-order retainer equivalence method is adopted to obtain the discrete expression of the controlled object as:

$$G(z) = \frac{7.416z + 5.655}{z^2 + 0.1847z + 0.436} \quad (32)$$

The contrast diagram of the step response of FOPID controller after discretization is presented in Figure 14.

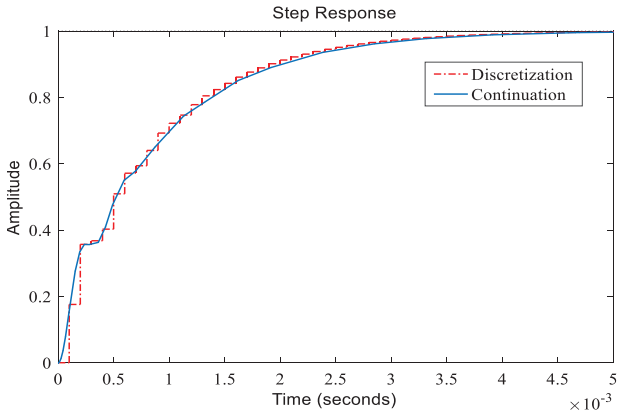

FIGURE 14. Step response of fractional order controller after discretization.

The Tustin method is adopted to discretize a TZTP compensator. When the sampling frequency is set to 200kHz, it just shows stable control effect still with a certain distortion. The discrete expression is shown as:

$$D_{TZTP}(z) = \frac{9.487z^3 - 8.67z^2 - 9.469z + 8.688}{z^3 - 0.2505z^2 - 0.6091z - 0.1404} \quad (33)$$

The differential equation of the TZTP compensator available for programming is also given by:

$$u(k) = 9.487e(k) - 8.67e(k-1) - 9.469e(k-2) + 8.688e(k-3) + 0.2505u(k-1) + 0.6091u(k-2) + 0.1404u(k-3) \quad (34)$$

where $u(k)$ and $e(k)$ represents the controller output and the error input signal respectively.

The contrast diagram of the step response of TZTP controller after discretization is shown in Figure 15.

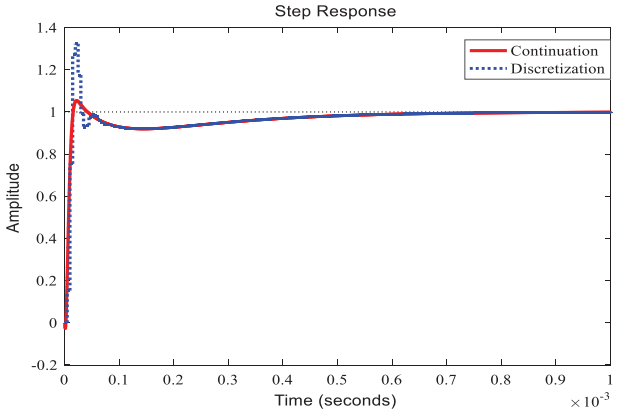

FIGURE 15. Step response of integer order controller after discretization.

VI. EXPERIMENTAL STUDY

The experimental setup of a 50W fuel cell stack and its peripheral devices is shown in Figure 16. Online parameter estimation and FOPID controller are performed on a laptop computer using Matlab. Three control scenarios are investigated: system starts to the rated load 24Ω, resistive load falls and rises under integer or fractional order control method. These scenarios provide a systematic way of demonstrating the effectiveness of the proposed controller for various situations of a change in the external load.

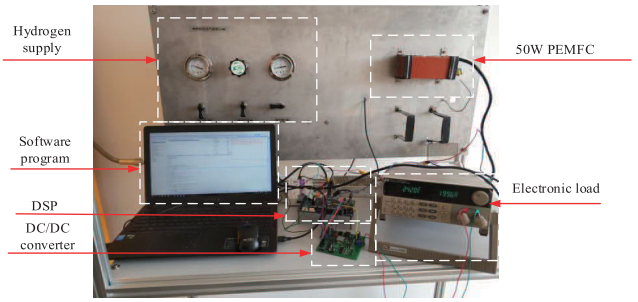

FIGURE 16. Experimental setup.

In order to make experimental results closer to the simulation waveform, parameters which are similar to those of simulation are adopted. Variation curve of resistive load is depicted in Figure 17, in which the resistive load starts at 24Ω, falls from 24Ω to 8Ω at 0.5s and shifts from 8Ω to 16Ω at 1s.

(1) When the system starts and approaches the rated load, the time response of the output voltage compensated by the fractional order controller is shown in Figure 18, while a corresponding response based on the integer order controller is depicted in Figure 19.

From Figure 18, it is found that the output voltage compensated by fractional order controller can reach a stable value smoothly with a peak value and a steady state value 24.1V respectively when system startup. And the ripple and peak are kept at about 0.2V. Furthermore, when considered from the perspective of peak overshoot, rise time and fall time of the

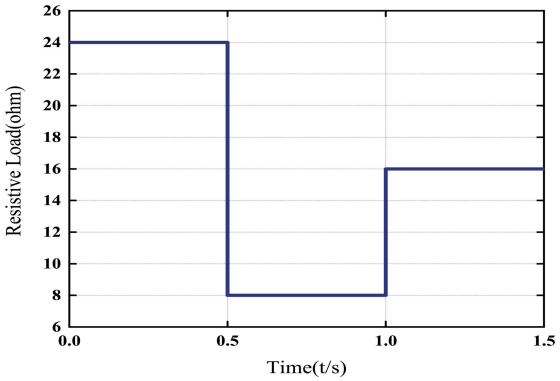

FIGURE 17. Variation curve of resistive load.

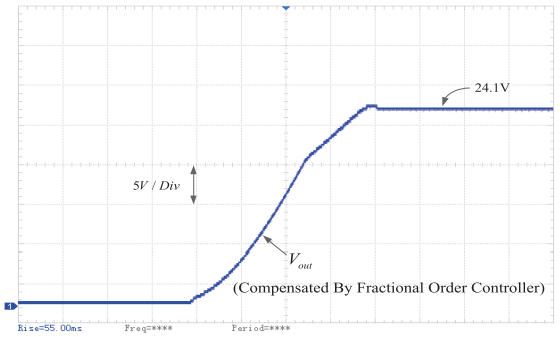

FIGURE 18. Output voltage when system startup with fractional order controller.

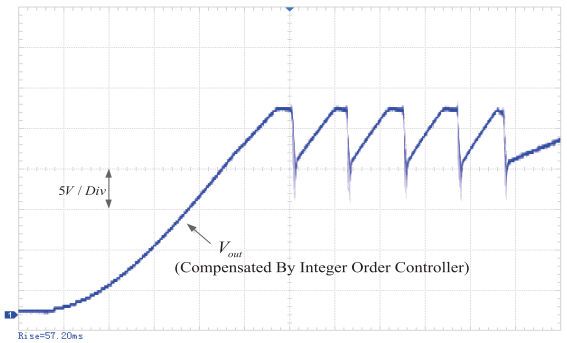

FIGURE 19. Output voltage when system startup with integer order controller.

output voltage are nearly 1.38ms when system startup with fractional order controller. Meanwhile, when system startup with integer order controller, rise time and fall time of the output voltage can reach 9.53ms and 2.38ms respectively.

Compared with the simulation process, the response time and ripple are increased, but the performance can satisfy the control requirement. However, the TZTP compensator with better performance in theory cannot stabilize the output voltage shown in Figure 19, which reflects that the fractional order controller has a better robustness in practical application.

(2) When the resistive load falls from 24Ω to 8Ω, the time response of the output voltage compensated by the fractional order controller is shown in Figure 20. In Figure 20, the output

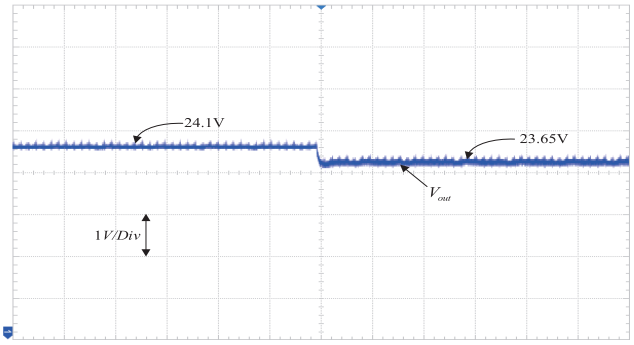

FIGURE 20. Output voltage at falling load with fractional order controller.

voltage decreases 0.45V (about 2%) in 5ms, and the ripple increases to 0.35V. Then a corresponding response based on the integer order controller is depicted in Figure 21. Compared with two figures, although the average value of the output voltage is almost the same, the ripples of voltage waveform with fractional and integer order controller are 0.11V and 0.39V respectively, which means output voltage with fractional order controller appears smaller ripple due to its good robustness.

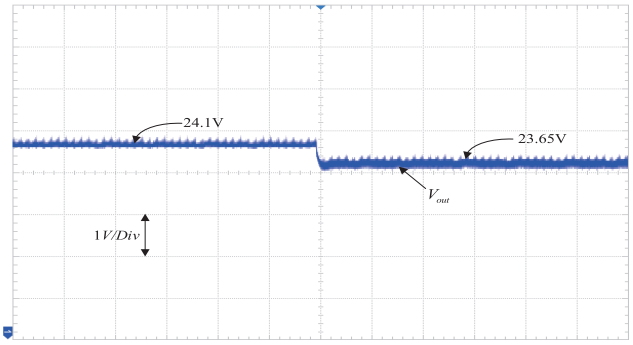

FIGURE 21. Output voltage at falling load with integer order controller.

(3) When the resistive load shifts from 8Ω to 16Ω, the time response of the output voltage compensated by fractional order controller is shown in Figure 22. The output voltage increases 0.7V in 5ms, and the ripple decreases to 0.15V. Then similarly, a corresponding response based on the integer order controller is depicted in Figure 23. Although the average value of the output voltage remains the same when compared with the result of fractional order controller, it is obvious that the waveform with integer order controller contains larger ripple.

Compared with the simulation process, it is obvious that the experimental results basically remain the same. Although the output voltage will transform with the change of the resistive load, its average value can be maintained at around 24V, thereby verifying the accuracy of simulation and experimental results.

Figure 24 presents the efficiency curve of the entire system compensated by a TZTP controller or FOPID controller when

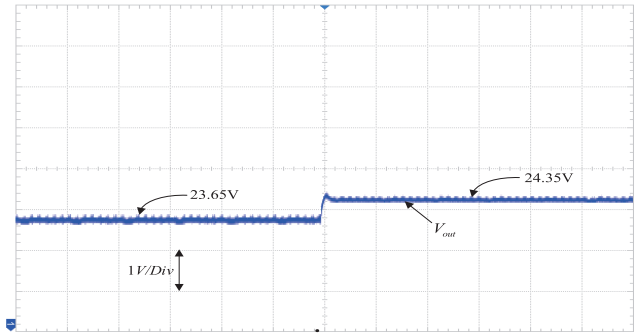

FIGURE 22. Output voltage at decreasing load with fractional order controller.

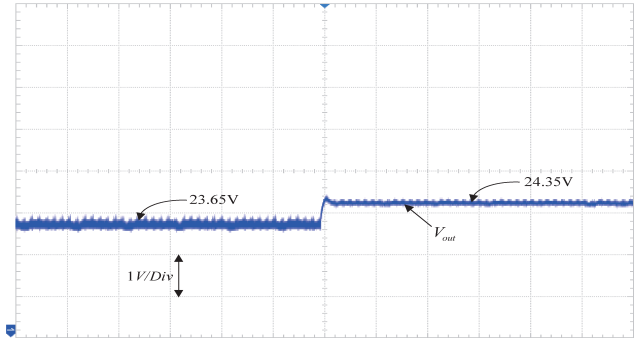

FIGURE 23. Output voltage at decreasing load with integer order controller.

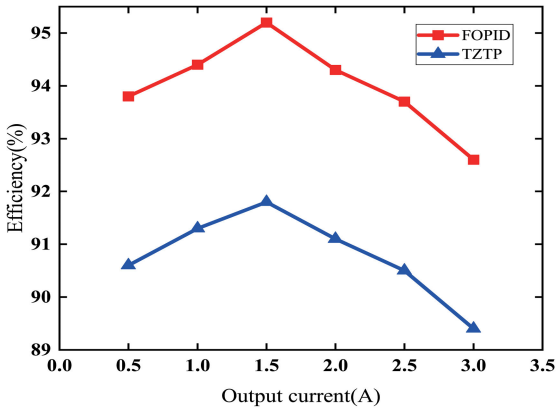

FIGURE 24. Efficiency curve of the entire system.

the output current varies between 0.5A and 3A. When the entire system reaches a stable state, it is obvious that the efficiency with a FOPID controller can remain above 92%, higher than that with a TZTP controller. Especially when the output current is 1.5A, the efficiency with a FOPID controller can even reach about 95.2%, which displays high effectiveness and stability of the whole system.

In summary, the power system response with FOPID control method retains almost zero overshoot, fast response speed and small ripple in the experiment. It is feasible to introduce the fractional order controller to the field of high frequency switching power supply. All the performance indexes of the pre-stage pre-stabilizing module of PEMFC can meet the design requirement.

VII. CONCLUSION

In this paper, a pre-stage DC-DC regulated voltage module for PEMFC power generation system is designed by using a FSBB converter. Based on the analysis of the working principle and the switch trigger strategy, a high frequency switching network equivalent model of this converter is established, then a two-zero/three-pole compensator and a fractional order PID controller are designed to realize stable output of the power system.

To reduce the inductor current ripple, a kind of dual-triggered switch strategy is employed in detail, and an accurate dynamic model of DC/DC converter is proposed for fuel cell measurement and control system. Then a fractional order PID controller is designed for voltage module compensation, in which a stochastic inertia weight PSO algorithm is employed to optimize parameters of this controller. Simulation and experiment results show that the designed DC-DC converter can fulfill the pre-regulator function effectively, and the dynamic response of system with fractional order PID controller has small overshoot, short settling time, small steady state ripple and acceptable error range. It is expected that the proposed fractional order control can be easily extended to more complex control problems with fractional characteristic, and could be applied to stationary and transportation systems, as well as low- and high-power fuel cell applications.

REFERENCES

[1] J. Jia, Y. Wang, Q. Li, Y. T. Cham, and M. Han, "Modeling and dynamic characteristic simulation of a proton exchange membrane fuel cell," *IEEE Trans. Energy Convers.*, vol. 24, no. 1, pp. 283–291, Mar. 2009.
[2] Y. Zhiyu, L. Tao, S. Qing, and L. Qi, "Design of generation controller of air-cooled self-humidifying proton exchange membrane fuel cell," *Trans. China Electrotech. Soc.*, vol. 33, no. 2, pp. 442–450, 2018.
[3] K. Shiluveru, A. Singh, A. Ahmad, and R. K. Singh, "Hybrid Buck–Boost multioutput quasi-Z-source converter with dual DC and single AC outputs," *IEEE Trans. Power Electron.*, vol. 35, no. 7, pp. 7246–7260, Jul. 2020.
[4] L. Liangjing, "Research on wide input passive lossless Buck-Boost converter," M.S. thesis, Shaanxi Univ. Technol., Hanzhong, China, 2019.
[5] L. Wenbo, "Three-port optical storage converter based on SiC devices," M.S. thesis, Xi'an Univ. Technol., Xi'an, China, 2019.
[6] L. Yafei, "Research on control strategy of non-inverting Buck-Boost bidirectional converter," M.S. thesis, Yanshan Univ., Qinhuangdao, China, 2018.
[7] Y. Z. Wangyu, "Design of programmable Buck-Boost DC/DC converter," *Mod. Electron. Technol.*, vol. 43, no. 4, pp. 29–33, 2020.
[8] S. Xiaofeng, Y. Ye, W. Baocheng, L. Xin, and P. Yao, "Zero-voltage switching three-level Buck-Boost bidirectional converter," *J. Elect. Eng. Technol.*, vol. 33, no. 2, pp. 293–300, 2018.
[9] X. Xiaoli, "Research and design of the system of wide input four-switch Buck-Boost converter," M.S. thesis, Chang'an Univ., Xi'an, China, 2019.
[10] R. W. Erickson, *Fundamentals of Power Electronics*, vol. 35, no. 1. Norwell, MA, USA: Kluwer, pp. 187–263.
[11] C. Zhanli, C. Weirong, D. Meiyu, and H. Guojun, "Dynamic characteristic analysis of PEMFC analysis and PID control," *Power Supply Technol.*, vol. 34, no. 4, pp. 338–341, 2010.
[12] Y. Haojie, X. Yan, W. Jinquan, and X. Lei, "Study of sliding mode control strategy for PEMFC-boost system," *Microcomput. Appl.*, vol. 36, no. 20, pp. 84–86 and 91, 2017.

[13] Z. Jun, Z. Lin, and Y. Meiwen, "Design of continuous model predictive controller for proton exchange membrane fuel cell," *Comput. Meas. Control*, vol. 27, no. 10, pp. 100–103 and 108, 2019.
[14] M. A. Taleb, O. Bethoux, and E. Godoy, "Identification of a PEMFC fractional order model," *Int. J. Hydrogen Energy*, vol. 42, pp. 1499–1509, Jan. 2017.
[15] C. Hongliang, "Research on modeling and thermal management of solid oxide fuel cell system," M.S. thesis, Huazhong Univ. Sci. Technol., Wuhan, China, 2008.
[16] Q. Zhidong, H. Yongkang, G. Weiping, and S. Qi, "Study on fractional nonlinear state space model of proton exchange membrane fuel cell," *Control Theory Appl.*, vol. 36, no. 3, pp. 86–93, 2019.
[17] L. Huili, Z. Xiaohua, and L. Wenguang, "Optimal $PI^{\lambda}D^{\mu}$ control of fractional buck converter," *Elect. Meas. Instrum.*, vol. 56, no. 16, pp. 134–141, 2019.
[18] C. Xiuhui, C. Yan, Z. Bo, J. Meng, and Z. Chunjiang, "Research on analysis and control performance of full fractional-order boost converter system," *J. Power Sources*, vol. 17, no. 6, pp. 27–33, 2019.
[19] Y. Chuan, "Buck-Boost converter suitable forwide input voltage range: Topologies and control strategies," M.S. thesis, Huazhong Univ. Sci. Technol., Wuhan, China, 2013.
[20] X.-Y. Ren, X.-B. Ruan, M.-Q. Li, H. Qian, and Q.-H. Chen, "Dual edge modulated four-switch Buck-Boost converter," *Proc. CSEE*, vol. 29, no. 12, pp. 16–23, 2009.
[21] D. Xu, *Modeling and Control of Power Electronic System*. Beijing, China: Machinery Industry Press, 2005, pp. 1–45.
[22] M. S. Bouakkaz, A. Boukadoum, O. Boudebbouz, N. Fergani, N. Boutasseta, I. Attoui, A. Bouraiou, and A. Necaibia, "Dynamic performance evaluation and improvement of PV energy generation systems using moth flame optimization with combined fractional order PID and sliding mode controller," *Sol. Energy*, vol. 199, pp. 411–424, Mar. 2020.
[23] B. N. Kommula and V. R. Kota, "Direct instantaneous torque control of brushless DC motor using firefly algorithm based fractional order PID controller," *J. King Saud Univ.-Eng. Sci.*, vol. 32, no. 2, pp. 133–140, Feb. 2020.
[24] C. Zhu and Y. Zou, "Summary of research on fractional-order control," *Control Decis.*, vol. 24, no. 2, pp. 161–169, 2009.
[25] I. Podlubny, "Fractional-order systems and controller," *IEEE Trans. Autom. Control*, vol. 44, no. 1, pp. 208–214, Jan. 1999.
[26] J. Kennedy and R. C. Eberhart, "Particle swarm optimization," in *Proc. IEEE Int. Conf. Neural Netw.* Piscataway, NJ, USA: IEEE Press, Nov./Dec. 1995, pp. 1942–1948.
[27] C. Xue, Z. Qi, M. Xu, and W. Ge, "Research on PEMFC fractional impedance characteristic modeling," in *Proc. Chin. Control Decis. Conf. (CCDC)*, Jun. 2018, pp. 3060–3065.
[28] W. Chun-Yang, L. Ming-Qiu, and J. Shu-Hua, *Design of Fractional Order Control System*. Beijing, China: National Defence Industy Press, 2014.

ZHIDONG QI was born in 1976. He received the Ph.D. degree in control theory and control engineering from Shanghai Jiao Tong University, in 2005. He was immersed in the fuel cell field for more than ten years. He is currently a Professor with the School of Automation, Nanjing University of Science and Technology. His main research interests include dynamic analysis of complex nonlinear of proton exchange membrane fuel cell, optimization of fuel cell performance, new theories, new methods and new technologies of modeling, and intelligent control of proton exchange membrane fuel cell.

JUNTAO TANG was born in 1997. He is currently pursuing the master's degree with the School of Automation, Nanjing University of Science and Technology. His main research interest includes power generation technology of proton exchange membrane fuel cell based on fractional calculus theory.

JIN PEI was born in 1995. He is currently pursuing the master's degree with the School of Automation, Nanjing University of Science and Technology. His main research interest includes power generation technology of proton exchange membrane fuel cell based on fractional calculus theory.

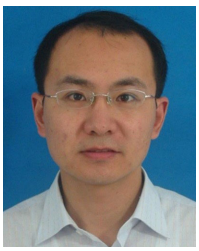

LIANG SHAN was born in 1979. He received the B.Sc. degree in electrical engineering and the Ph.D. degree in control science and control engineering from the Nanjing University of Science and Technology, China, in 2002 and 2007, respectively. He is currently a Professor with the Nanjing University of Science and Technology. His research interests include intelligence control algorithm, nonlinear systems, and control methods of motor servo systems.